

EUR 2994.e

EUROPEAN ATOMIC ENERGY COMMUNITY - EURATOM

RESOLUTION,
EFFICIENCY AND BACKGROUND EFFECTS
IN SEMICONDUCTOR SANDWICH FAST
NEUTRON SPECTROMETERS

by

R. A. RYDIN

1966



Joint Nuclear Research Center
Ispra Establishment - Italy

Chemistry Department
Nuclear Chemistry

LEGAL NOTICE

This document was prepared under the sponsorship of the Commission of the European Atomic Energy Community (EURATOM).

Neither the EURATOM Commission, its contractors nor any person acting on their behalf :

Make any warranty or representation, express or implied, with respect to the accuracy, completeness, or usefulness of the information contained in this document, or that the use of any information, apparatus, method, or process disclosed in this document may not infringe privately owned rights ; or

Assume any liability with respect to the use of, or for damages resulting from the use of any information, apparatus, method or process disclosed in this document.

This report is on sale at the addresses listed on cover page 4

at the price of FF 6,—	FB 60	DM 4.80	Lit. 750	Fl. 4.30
------------------------	-------	---------	----------	----------

When ordering, please quote the EUR number and the title, which are indicated on the cover of each report.

This document was reproduced on the basis of the best available copy.

Printed by Vanmelle
Brussels, June 1966

EUR 2994.e

EUROPEAN ATOMIC ENERGY COMMUNITY - EURATOM

RESOLUTION,
EFFICIENCY AND BACKGROUND EFFECTS
IN SEMICONDUCTOR SANDWICH FAST
NEUTRON SPECTROMETERS

by

R. A. RYDIN

1966



Joint Nuclear Research Center
Ispra Establishment - Italy

Chemistry Department
Nuclear Chemistry

SUMMARY

Four separate areas related to semiconductor sandwich spectrometer response were analysed, making extensive use of digital computer calculations. These were :

- 1) *Characteristic resolution response function for monoenergetic neutrons.*

Response functions were calculated for various layer thicknesses of Li^6F and gold at a number of different energies. Results compare favorably with existing experimental data.

- 2) *Relative detection efficiency vs neutron energy.*

The relative detection efficiency, for detection of the reaction products in coincidence, was calculated for both He^3 and Li^6 spectrometers as a function of detector orientation angle. The effect is found to be significant, especially for the He^3 spectrometer.

- 3) *Effects of non-gaussian detector response.*

Spectrum unfolding techniques are essentially not necessary for Li^6 spectrometers above 0.5 MeV, but it was found that care must be taken to correctly interpret the absolute detection efficiency of the detector.

- 4) *True coincidence background response.*

The true coincidence background response, due to reactions occurring in the silicon of the diodes, was calculated for the case of an incident Pu- α -Be neutron spectrum. The background was found to be due primarily to the ground state (n,p) and (n, α) reactions. The results are in good agreement with available experimental data.

TABLE OF CONTENTS.

- I. Introduction
- II. The Characteristic Resolution Function of a Li^6F Semiconductor Sandwich Spectrometer
 - 2.1 General
 - 2.2 Energy Loss Equations
 - 2.3 Resolution Function Calculation
 - 2.4 Results
 - 2.5 Conclusions
- III. The Relative Detection Efficiency of Semiconductor Sandwich Spectrometers.
 - 3.1 General
 - 3.2 Coincidence Detection Probability
 - 3.3 Relative Detection Efficiency Calculation
 - 3.4 Results
 - 3.5 Conclusions
- IV. The Effect of a Non-Gaussian Response Function on Li^6F Semiconductor Sandwich Spectrometer Results
 - 4.1 General
 - 4.2 The Response Function
 - 4.3 Results
 - 4.4 Conclusions
- V. True Coincidence Background Response of a Semiconductor Sandwich Spectrometer
 - 5.1 General
 - 5.2 Background Calculation
 - 5.3 Results and Conclusions

Acknowledgement

Bibliography

LIST OF FIGURES

- Figure 1. Charged Particle Energy Loss Rates for Li^6F .
- Figure 2. Charged Particle Energy Loss Rates for Gold.
- Figure 3. Diagram for Characteristic Resolution Function Calculations.
- Figure 4. Loss Distribution Probabilities vs Energy Loss, for Thermal Neutrons.
- Figure 5. Relative Loss Distribution Curves for Various Detectors, for Thermal Neutrons.
- Figure 6. Comparison Between Theoretical and Experimental Resolution Curves, for Thermal Neutrons.
- Figure 7. Loss Distribution Probabilities vs Energy Loss, for 8 MeV Neutrons.
- Figure 8. Relative Loss Distribution Curves for Various Neutron Energies.
- Figure 9. Diagram for Relative Detection Efficiency Calculations.
- Figure 10. Conditional Detection Probability Curves for Various Detector Orientations, for 10 MeV Neutrons.
- Figure 11. Triton Emission Probability Curve, for 14 MeV Neutrons.
- Figure 12. Relative Detection Efficiency Curves for a Li^6 Detector, for No Discrimination of Thermal Neutron Events.
- Figure 13. Relative Detection Efficiency Curves for a Li^6 Detector, for a Discriminator Set at 2.1 MeV.
- Figure 14. Relative Detection Efficiency Curves for a He^3 Detector with Zero Loss Angle, for No Discrimination of Thermal Neutron Events.

- Figure 15. Relative Detection Efficiency Curves for a He^3 Detector with a 5° Loss Angle, for No Discrimination of Thermal Neutron Events.
- Figure 16. Relative Detection Efficiency Curves for a He^3 Detector with a 10° Loss Angle, for No Discrimination of Thermal Neutron Events.
- Figure 17. Relative Detection Efficiency Curves for a He^3 Detector with Zero Loss Angle, for a Discriminator Set at 0.2 MeV.
- Figure 18. True Spectrum vs Detected Spectrum, for a Detector with a Gaussian Response.
- Figure 19. True Spectrum vs Detected Spectrum, for a Detector with a Non-Gaussian Response.
- Figure 20. Comparison of the Coincidence Background Response to the True Neutron Spectrum Response of the Spectrometer, Calculated Data (Pu- α -Be Spectrum Neutrons)
- Figure 21. Comparison of the Coincidence Background Response to the True Neutron Spectrum Response of the Spectrometer, Available Experimental Data (Pu- α -Be Spectrum Neutrons)

I. INTRODUCTION (°)

Semiconductor sandwich spectrometers are constructed by placing a neutron sensitive layer between two closely spaced surface barrier detectors. The charged particles produced in the neutron reaction are usually detected in coincidence and their energies electronically added together. The neutron energy can thus be deduced from the sum of the particle energies minus the Q value of the reaction, and the use of a positive Q value reaction helps to discriminate against interfering background reactions. The major advantage of these spectrometers is their approximately gaussian response to monoenergetic neutrons which is essentially linear with energy. The major disadvantage is low efficiency.

At the present time there exists a relatively large amount of experimental information obtained with both He^3 and Li^6F semiconductor sandwich spectrometers. Unfortunately, the theoretical analysis of these devices has not kept pace with the experimental work, and, therefore, although most effects have been qualitatively explained, quantitative information has been lacking.

There exist essentially four major areas of darkness. The first is the prediction of the characteristic resolution function of the device as a function of the properties of the sensitive layer. The second is the prediction of the variation of efficiency with energy due to the loss of events which fail to produce a coincidence. The third is the problem of unfolding the spectrometer data to obtain the true incident spectrum, and in particular, determining the effects of non-gaussian detector response.

And the last is the prediction of the background response of the detector due to (n,p) and (n,α) reactions occurring in the silicon of the diodes.

These problem areas are the subject of this paper.

II. THE CHARACTERISTIC RESOLUTION FUNCTION OF A Li⁶F SEMICONDUCTOR SANDWICH SPECTROMETER.

2.1 General.

The characteristic resolution function of a semiconductor sandwich spectrometer is considered to be the detector response curve for incident monoenergetic neutrons which is produced entirely by the physical processes in the detector, (energy losses in the Li⁶F and gold layers plus the coincidence requirement) neglecting statistical smoothing brought about by straggling, electronic noise, etc. A careful literature search reveals only one attempt to calculate this function,^(1,2) and the preliminary result given there appears to be in doubt. In this work, we have adopted the same initial formulation as the previous work⁽¹⁾ but modify the final equations and calculational procedure to obtain a more straightforward solution. Only the simplest case, that of a neutron beam perpendicularly incident on a semi-infinite sandwich, is considered, since the general case⁽²⁾ requires an extra integration which would use a great deal of computer time.

2.2 Energy Loss Equations.

Following Reference 1, we assume that the particles travel in straight line paths and lose energy, in passing through the gold and Li⁶F layers of the detector, at a constant rate which is determined by the initial energy of the particle (or the initial energy minus a small average energy loss) according to the equation,

$$-\frac{dE}{dx} = \epsilon(E_{\text{initial}}) \left(\frac{\text{MeV}}{\text{mg/cm}^2} \right) \quad (1)$$

The quantity $\epsilon(E)$ is required for each material and each particle type. We use the following subscripts to denote these functions,

$$\begin{aligned}
 \epsilon_{\alpha L} &= \text{loss rate of an alpha particle in Li}^6\text{F} \\
 \epsilon_{tL} &= \text{loss rate of a triton in Li}^6\text{F} \\
 \epsilon_{\alpha A} &= \text{loss rate of an alpha particle in gold} \\
 \epsilon_{tA} &= \text{loss rate of a triton in gold}
 \end{aligned}
 \tag{2}$$

The required quantities can be calculated using a form of the Bethe-Bloch equation,^(3,4,5) which is,

$$-\frac{dE}{dx} = \frac{4\pi e^4 z^2}{m_o V^2} NB
 \tag{3}$$

where N is given in atoms/mg. The stopping power, B, is defined for the non-relativistic case, neglecting non-participation corrections, as,

$$B = Z \ln \left(\frac{2m_o V^2}{I} \right)
 \tag{4}$$

The following ionization potentials were utilized in the calculations,⁽³⁾

$$\begin{aligned}
 I_{\text{Au}} &= 810 \quad \text{eV} \\
 I_{\text{F}} &= 108 \quad \text{eV} \\
 I_{\text{Li}^6} &= 36 \quad \text{eV}
 \end{aligned}
 \tag{5}$$

A simple additivity law is used for compounds,^(3,4) so that the stopping power for Li⁶F is,

$$B_{\text{Li}^6\text{F}} = \frac{1}{2} B_{\text{Li}^6} + \frac{1}{2} B_{\text{F}}
 \tag{6}$$

For gold, the Bethe-Bloch equation is not valid for low energy particles,⁽⁴⁾ and, hence, we must make use of experimental data to obtain that part of the curve. The resulting loss rate curves are shown in Figures 1 and 2. Note that a part of the gold curve is drawn in, in order to connect the calculated and experimental curves. However, the energy losses in the gold are small compared to the losses in the Li^6F , and, hence, inaccuracies in the gold curves are not too influential on the final results.

2.3 Resolution Function Calculation.

The one dimensional model chosen to represent the detector is shown in Figure 3. It consists of two diodes, each having a gold surface layer $D \mu\text{g}/\text{cm}^2$ thick, which surround a Li^6F layer $T \mu\text{g}/\text{cm}^2$ thick. A neutron enters on the z axis, and produces an (n,T) reaction at depth z in the Li^6F layer which results in a triton being emitted at an angle θ from the z axis. The probability of having a triton emitted at an angle θ can be computed from the differential angular cross section and the kinematics of the reaction⁽⁶⁾. By virtue of the conservation laws, the angle ϕ is then uniquely determined as well as the energies of both the alpha particle and triton.⁽⁷⁾

The total energy loss is the sum of the losses of the two particles emitted in the (n,T) reaction. If we exclude those cases where the alpha particle and the triton are both detected by the same diode, and hence do not meet the coincidence requirement, then the detector loss equations can be written in the following form⁽¹⁾,

$$\underline{\theta \leq 90^\circ}$$

$$\Delta E(E_n, \theta) = \frac{\epsilon_{tL}(T-z) + \epsilon_{tA} D}{\cos \theta} + \frac{\epsilon_{\alpha L} z + \epsilon_{\alpha A} D}{|\cos \phi|} \quad (7)$$

and,

$$\underline{\theta \geq 90^\circ}$$

$$\Delta E(E_n, \theta) = \frac{\epsilon_{tL} z + \epsilon_{tA} D}{|\cos \theta|} + \frac{\epsilon_{\alpha L}(T-z) + \epsilon_{\alpha A} D}{\cos \phi} \quad (8)$$

Note that the ϵ 's are a function of θ since the initial energies of the particles are determined by the neutron energy E_n , and by the emission angle θ .

Since these equations are linear in z , we need only calculate the maximum and minimum values at $z = 0$ and $z = T$, or vice versa, and assume a uniform distribution between.

These extreme values can be obtained from the following expressions,

$$\Delta E(E_n, \theta)_{\min} = \frac{\epsilon_{tL} T + \epsilon_{tA} D}{|\cos \theta|} + \frac{\epsilon_{\alpha A} D}{|\cos \phi|} \quad (9)$$

and,

$$\Delta E(E_n, \theta)_{\max} = \frac{\epsilon_{tA} D}{|\cos \theta|} + \frac{\epsilon_{\alpha L} T + \epsilon_{\alpha A} D}{|\cos \phi|} \quad (10)$$

The resolution function for the detector is obtained by suitably summing the energy loss distributions calculated above, weighted by the probability of emission of a triton at an angle θ and by the probability of detection of the event in coincidence, over all possible values of θ .

The emission probability for a reaction with a neutron of energy E_n has been calculated previously⁽⁶⁾ in the form,

$$p_e(E_n, \theta) d\theta = 2\pi \sin \theta \left(\frac{d\sigma(E_n, \theta)}{d\Omega_{lab}} \right)_{\text{normalized}} d\theta \quad (11)$$

where by definition,

$$\int_0^\pi p_e(E_n, \theta) d\theta = 1.0 \quad (12)$$

Due to the geometrical coincidence detection conditions, as formulated in Reference 6, not all events are recorded by the spectrometer. If $p_D(E_n | \theta)$ is this probability, which has a value of either 0 or 1, then the detected emission probability is given by,

$$p_{\text{Det}}(E_n, \theta) = p_e(E_n, \theta) \cdot p_D(E_n | \theta) \quad (13)$$

Now, we consider that each angle θ gives rise to a uniform distribution of losses between $\Delta E(E_n, \theta)_{\min}$ and $\Delta E(E_n, \theta)_{\max}$ as we cross the Li^6F layer. The total number of events appearing in this energy range must equal the number produced and recorded at θ , hence,

$$\int_{\Delta E(E_n, \theta)_{\min}}^{\Delta E(E_n, \theta)_{\max}} p_{\text{Dt}}(\Delta E, E_n, \theta) dE d\theta = p_{\text{Det}}(E_n, \theta) d\theta \quad (14)$$

This leads to a definition of the joint detected loss probability $p_{Dt}(\Delta E, E_n, \theta)$, which is,

$$p_{Dt}(\Delta E, E_n, \theta) d\theta = \frac{p_{Det}(E_n, \theta) d\theta}{\Delta E(E_n, \theta)_{\max} - \Delta E(E_n, \theta)_{\min}} \quad (15)$$

If either particle losses all of its energy in the gold and Li⁶F layers, it cannot be counted in coincidence. We correct for this effect by cutting the energy loss distribution, equations (7) and (8), at the point where all of the energy of this particle is lost, and, hence, compute a modified maximum energy loss, $\Delta E(E_n, \theta)_{\max \text{ mod}}$, to replace that of Equation (10). This new maximum loss value is equal to all of the first particle's energy plus the amount of the second particle's energy lost at the position of total loss of the first. The joint detected loss probability, Equation (15), is set to zero for a ΔE lying outside of the range $\Delta E(E_n, \theta)_{\max}$ (or $\Delta E(E_n, \theta)_{\max \text{ mod}}$) to $\Delta E(E_n, \theta)_{\min}$.

Finally, the resolution function for a neutron of energy E_n , which is equal to the energy loss probability distribution, is obtained by integration of the joint detected loss probability over all possible triton emission angles.

The result is,

$$N(E_n, \Delta E) dE = \int_0^{\pi} p_{Dt}(\Delta E, E_n, \theta) d\theta dE \quad (16)$$

We note in passing that,

$$\int_0^{\infty} N(E_n, \Delta E) dE \leq 1.0 \quad (17)$$

since not all events are detected in coincidence.

2.4 Results.

A computer program was written in Fortran IV for the IBM 7090 in order to solve this problem. Representative results of the above calculations are given in Figures 4 to 8 where resolution functions are shown for various neutron energies and absorbing layer thicknesses.

Figure 4 shows a result for thermal neutrons incident on a detector having $150 \mu\text{g}/\text{cm}^2$ of Li^6F , and $100 \mu\text{g}/\text{cm}^2$ of gold on each diode. Since the alpha particle and triton are emitted back to back in this case, the emission and detection probabilities are symmetric and essentially all particles are detected in coincidence. As the emission angle approaches 90° , the amount of energy lost increases greatly and these events give rise to a tail on the distribution.

Figure 5 shows the same situation for various Li^6F and gold layer thicknesses. It is apparent that the gold is not too influential on the resolution function, but that the Li^6F layer is very important. An increase in the Li^6F layer from $150 \mu\text{g}/\text{cm}^2$ to $250 \mu\text{g}/\text{cm}^2$ increases the predicted full width at half maximum (FWHM) from 270 to 450 KeV and the most probable energy loss from 250 to 400 KeV. At the same time, the tail becomes relatively more important.

Obviously, the results are sensitive to the constants used in the calculations. To the extent that these are in doubt and to the extent that the experimental data is modified by the experimental arrangement and electronic system, the results cannot be absolutely compared to experiment. On the other hand, the results are of the right

order of magnitude and the shape of the predicted resolution curve, including the fraction appearing in the tail, agrees quite well with available experimental data,^(8,9) as can be seen in Figure 6. The calculations are valuable, therefore, to the extent that they allow one to understand the phenomena involved and to predict the effect of a change in the experimental configuration.

Figure 7 shows a result for 8 MeV neutrons. Due to the forward distribution of particles in the laboratory system, there exists a range of emission angles (see inset) where no detection in coincidence is possible. There also exists a band of rather narrow energy loss values ($\theta > 90^\circ$) which can be explained by the fact that the forward directed alpha particles, detected in coincidence, all travel in a rather small cone about the z axis, hence losing a minimum amount of energy. As a consequence, the calculated loss distribution curve contains a discontinuity.

Results for three different energies are shown in Figure 8. Also presented is an experimental curve taken from Reference 8, which, if studied carefully, indicates the presence of a discontinuity which the authors ignored when drawing a curve through their experimental points. This would appear to qualitatively verify the calculations.

2.5 Conclusions.

Conclusions which can be reached as a result of this study are the following:

- 1) The calculational model chosen appears to be adequate to qualitatively predict the resolution function of a Li^6F sandwich spectrometer;

- 2) The predicted FWHM is almost constant with neutron energy, decreasing slightly as the neutron energy increases;
- 3) The minimum possible energy loss decreases somewhat with increasing neutron energy;
- 4) The average energy loss decreases somewhat with increasing neutron energy;
- 5) The tail becomes relatively more important as the Li^6F thickness increases; and,
- 6) The distributions should vary somewhat with changes in detector orientation since the loss contributions would be weighted with different probabilities.

III. RELATIVE DETECTION EFFICIENCY OF A SEMICONDUCTOR SANDWICH SPECTROMETER.

3.1 General.

Since the time of the early experiments,^(8,9) it has been recognized that the detection efficiency of a semiconductor sandwich spectrometer should vary with energy (in addition to the cross section variation) due to the fact that both reaction products do not always enter different diodes and hence do not meet the coincidence requirement for detection. This effect, which can be called the relative detection efficiency, is not a simple function to calculate. In particular, it depends upon the following variables: 1) the differential angular cross section; 2) the reaction kinematics; 3) The detector orientation with respect to the incoming neutrons; 4) The size and shape of the detector diodes; 5) The diode spacing; and, 6) The size and position of the sensitive layer.

The first three variables basically account for the shape of the relative detection efficiency curve as a function of energy, and are the easiest to take into account in a calculation. The last three produce a geometrical edge effect which is difficult to include exactly. The approach taken here is heuristic in nature: the edge effects are approximated by an "average loss angle" which can be estimated or calculated for a given detector configuration, and; the relative detection efficiency is calculated as a function of a "loss angle" parameter using an idealized model.

3.2 Coincidence Detection Probability.

The model chosen to represent the spectrometer is shown in Figure 9. It is basically a semi-infinite sandwich, tilted to the direction of the incoming neutrons by an orientation angle α , which has in addition a loss angle δ in which no charged particles can be recorded. The triton is emitted at an angle θ from the neutron direction and the alpha particle at an angle ϕ from the neutron direction.

The derivation is similar to that given in Reference 6. Considering β as a rotation angle about the neutron direction, which has a uniform probability of occurring and defines the plane in which the charged particles are emitted, the coincidence conditions can be written in the following manner,

$$\begin{aligned}
 & \text{if } \arctan \left[\frac{\tan(90^\circ + \alpha)}{\cos \beta} \right] - \delta > \theta > 0^\circ \\
 & \text{then } 180^\circ > \phi > \delta + \arctan \left[\frac{\tan(90^\circ - \alpha)}{\cos \beta} \right] \\
 & \text{or if } 180^\circ > \theta > \delta + \arctan \left[\frac{\tan(90^\circ + \alpha)}{\cos \beta} \right] \\
 & \text{then } \arctan \left[\frac{\tan(90^\circ - \alpha)}{\cos \beta} \right] - \delta > \phi > 0^\circ
 \end{aligned} \tag{18}$$

Given a neutron energy, E_n , and a triton emission angle, θ , the alpha particle emission angle, ϕ , and the energy of the alpha particle and triton can be calculated. The coincidence detection probability for a given orientation angle, α , is then computed numerically from the following integral,

$$p_D(E_n | \theta, \alpha, \delta) = \frac{1}{\pi} \int_0^\pi \left[\begin{array}{l} \text{Detection conditions} \\ \text{given } E_n, \theta, \alpha, \delta, \text{ and } \beta \end{array} \right] d\beta \tag{19}$$

A result of this calculation for the $\text{Li}^6(n,T)\text{He}^4$ reaction is shown in Figure 10.

If a low level discriminator is used, the above expression can be modified in the manner of Reference 11 to omit detection whenever either the alpha particle or triton energy fall below the discriminator threshold setting.

The result is,

$$p_D(E_n | \theta, \alpha, \delta, E_{DISC}) = \frac{1}{\pi} \int_0^{\pi} \left[\begin{array}{l} \text{Detection conditions} \\ \text{given } E_n, \theta, \alpha, \delta, E_{DISC} \\ \text{and } \beta \end{array} \right] d\beta \quad (20)$$

3.3 Relative Detection Efficiency Calculations.

The relative detection efficiency as a function of E_n , α , δ , and E_{DISC} can now be calculated. It is equal to the integral of the coincidence detection probability, Equation (20), weighted by the probability of emission of a triton calculated from Equation (11) (an example of the emission probability for the $Li^6(n,T)He^4$ reaction is shown in Figure 11), taken over all possible values of θ . The result is,

$$\epsilon_R(E_n, \alpha, \delta, E_{DISC}) = \int_0^{\pi} p_e(E_n, \theta) \cdot p_D(E_n | \theta, \alpha, \delta, E_{DISC}) d\theta \quad (21)$$

3.4 Results.

For the $Li^6(n,T)He^4$ reaction, a Q value of 4.78 MeV was used and differential angular cross section data, taken from Reference 12, were converted to the laboratory system following the method of Reference 6. For the $He^3(n,p)T$ reaction, a Q value of 0.764 MeV was used and the differential cross sections were assumed to be isotropic in the center of mass system.

Results of the relative detection efficiency calculations are given for the Li^6F spectrometer in Figures 12 and 13, for the case of zero loss angle.

When the discriminator is set so that all neutron events are recorded, the relative detection efficiency curves, as a function of orientation angle, decrease smoothly with increasing energy. The efficiency for neutrons perpendicularly incident on the sensitive layer is markedly less than for parallel incidence, which is in qualitative agreement with the "almost twice" result for 14 MeV neutrons reported in Reference 10. Values for intermediate orientations are given, so that, if the angular neutron distribution in an actual experiment is approximately known, an average relative detection efficiency can easily be calculated.

When the discriminator is set at ~ 2.1 MeV, all of the alpha particle pulses produced by thermal neutrons fail to pass the discriminator. Hence, all of the thermal neutron caused events are ignored by the electronics and true pulse pileup effects in the slow electronic circuits can be minimized.⁽¹¹⁾

However, when the discriminator is set to this value, some true coincidences at higher energies are lost⁽¹¹⁾. The resulting relative detection efficiency curves for this case are shown in Figure 13.

Results for the He^3 spectrometer are given in Figures 14 to 17. As in the case of the Li^6F spectrometer, the relative detection efficiency curves for the condition of no thermal neutron discrimination decrease smoothly with increasing energy.

The major variation occurs below about 2 MeV and the curves are relatively constant above this energy. It is interesting

to note that the difference between parallel and perpendicular incidence is even more marked for He^3 than for Li^6F because the reaction is more forward directed in the laboratory system. In this case, the difference is more than a factor of two at 14 MeV.

As the loss angle is increased, the relative detection efficiency decreases. As a rough approximation, for any given orientation angle, this effect is linearly proportional to the loss angle. Therefore, for relatively closely spaced detector diodes, it would seem approximately valid to calculate an average loss angle from geometrical considerations and to use this to obtain an "edge effect" correction from the curves.

When the discriminator is set at 0.2 MeV, which discriminates against all tritons produced by thermal neutron events, the relative detection efficiency curves are modified as shown in Figure 17. It is interesting to note that, for any given orientation angle, the predicted relative detection efficiency is almost constant with energy above 1 MeV.

3.5 Conclusions.

The following conclusions can be drawn as a result of this work:

- 1) The relative detection efficiency represents a significant absolute calibration effect, even for thermal neutrons if the average loss angle is appreciable;
- 2) The relative detection efficiency represents a significant relative effect as a function of energy. There exist some data on Pu- α -Be sources, taken with $\text{He}^{3(13)}$ and $\text{Li}^6\text{F}^{(14)}$ spectrometers which were not corrected for the relative detection efficiency variation;

- 3) It is important to know the angular neutron distribution if absolute flux determinations must be performed;
- 4) There may be significant experimental advantages to operating the spectrometer at a discriminator level which excludes thermal neutron events and hence minimizes true pulse pileup in the slow electronic circuits;⁽¹⁵⁾
- 5) It would be valuable to experimentally check the relative detection efficiency curves.

IV: THE EFFECT OF A NON-GAUSSIAN RESPONSE FUNCTION ON
Li⁶F SEMICONDUCTOR SANDWICH SPECTROMETER RESULTS.

4.1 General.

A semiconductor sandwich spectrometer has a response function which, to a reasonable approximation, is a gaussian plus a low energy tail. The width of the gaussian, which is of the order of 150 to 300 KeV for practical spectrometers, is found both experimentally and theoretically to be essentially constant over a range from thermal energy to >14 MeV neutrons. The detectors are found to respond linearly with respect to neutron energy.

It is of interest to know the effect of the finite resolving power of these devices upon the experimental results for various spectra which we wish to measure. The method chosen here is to assume a reasonable form for the response function of the detector and then to compare given input spectra to the results obtained when the spectra are "smeared" by the response function. Although this approach may appear to be somewhat simple minded, it can lead to an important understanding of the manner in which these spectrometers function and thus help in the interpretation of actual experimental data.

4.2 The Response Function.

The response function is chosen to be a variable resolution width gaussian plus a low energy tail which starts from a given percentage of the peak height and goes linearly to zero. This choice for a tail has the disadvantage that

the percentage of neutrons in the tail slowly increases as the neutron energy increases. However, the model is relatively easy to analyse.

We define E as the summed particle energy, which is the sum of the neutron energy, E_n , and the Q value of the reaction.

We further define E' as the detected energy, F as the tail fraction at the center of the gaussian peak, and FWHM as the resolution width of the gaussian. Then, the normalized kernel can be written,

$$G(E', E) = \frac{\exp\left[-\left(\frac{1.665(E' - E)}{\text{FWHM}(E)}\right)^2\right] + \frac{FE'}{E} \Big|_{E' \leq E}}{\frac{\text{FWHM}(E)}{0.9394} + \frac{FE}{2}} \quad (22)$$

Considering the true response to be the product of the neutron spectrum and the Li^6 cross section,

$$R(E) = \sigma(E_n) \phi(E_n) \quad (23)$$

we can then write an expression for the detected response, which is,

$$D(E') = \int_0^{\infty} R(E) G(E', E) dE \quad (24)$$

This can be solved by a numerical approximation which is essentially equivalent to the trapezoidal rule,

$$D(E') \approx \sum_i R_i G_i(E') \Delta E_i \quad (25)$$

4.3 Results.

Results for a fission spectrum plus a thermal neutron component are given in Figure 18 for the case of a pure gaussian response curve and in Figure 19 for the exaggerated case of a gaussian plus a tail which reaches 10% of the peak height.

Three distinct effects may be noted. First, the input and output spectral shapes essentially agree with each other in the region where the spectrum varies slowly in the space of a resolution width regardless of whether the resolution is taken to be 150 KeV, 300 KeV, or a variable between these limits. Second, the shapes deviate from each other near the Li^6 cross section resonance, and the resonance cannot be readily distinguished from the thermal peak unless the thermal plus epithermal component is small, which is unlikely in a real experiment. Finally, the main effect of the tail is to cause the measured spectrum to fall below the input spectrum by an amount approximately equal to the fraction of events appearing in the tail.

4.4 Conclusions.

The conclusions which can be made as a result of this work are the following;

- 1) The experimental curve will always be distorted in the region between thermal neutron energy and the Li^6 cross section resonance at 250 KeV. It will be relatively impossible to avoid having a "thermal neutron" component because of the

interaction between the $1/v$ cross section and any slowing down spectrum above the cadmium cut-off. An unfolding scheme⁽¹⁶⁾ may or may not be useful in this region;

- 2) The experimental curve should follow the shape of the true spectrum, $R(E)$, faithfully as long as the true spectrum does not change rapidly in an energy interval of the order of a resolution width;
- 3) The experimental curve will lie under the true spectrum by an amount essentially equal to the fraction of events appearing in the non-gaussian part of the response curve.
Unless care is taken to correctly interpret this effect, it may be mistakenly explained as an absolute calibration discrepancy;
- 4) Unfolding procedures should not be necessary above an energy of ~ 0.5 MeV for fission type spectra or for spectra similar to that from a Pu- α -Be source.

V. TRUE COINCIDENCE BACKGROUND RESPONSE OF A SEMICONDUCTOR SANDWICH SPECTROMETER.

5.1 General.

A true coincidence background count occurs when a proton or an alpha particle, emitted in an (n,p) or (n,α) reaction in silicon, crosses both diodes and deposits enough energy in each to produce coincident pulses above a predetermined discriminator level. Since the Q values for these background reactions are negative, while those for the Li^6 or He^3 detection reactions are positive, a reaction with a given energy neutron will record a background count in a much lower channel than a true count, the offset being equal to the difference in the Q values. If the particles do not lose all of their energy in the depletion regions, then the background count will be recorded in a still lower channel.

Since silicon reactions are possible which proceed from various excited levels of the residual nuclei, these excited states must be taken into account. This is done by considering each as a separate reaction with its own cross section curve (excited level cross section data are given in the Brookhaven compilation⁽¹⁷⁾), and its own Q value equal to the ground state Q value minus the energy of the excited level.

5.2 BACKGROUND CALCULATION.

The calculational procedure is essentially identical to that given in a previous paper⁽¹¹⁾ with the exception that the excited levels are considered separately. The assumptions made are the following:

- 1) The detector is a semi-infinite sandwich (one dimensional calculation);
- 2) There are no losses in the sensitive layer or dead layers of the detector;
- 3) The particles are emitted isotropically in the laboratory system.

With these assumptions, the coincidence background rate at any summed particle energy for a given input spectrum is computed by integrating over the entire possible source volume of silicon. The equation used is the following,

$$N(E_s) = R_{Ti}(E_n) \pi/2 \int_0^\infty dE_n \sum_i \left[\Sigma_i(E_n) \phi(E_n) \int_0^x dx \int_0^{\pi/2} d\theta \left(\frac{\sin \theta}{2} \right) p_s(E_s | x, \theta, R_{Ti}, DL, DISC) \right] \quad (26)$$

where: $N(E_s)$ is the coincidence background detection rate at a given summed particle energy,

E_s (number) ;
 $\text{cm}^2\text{-sec-MeV}$

$\Sigma_i(E_n)$ is the macroscopic absorption cross section⁽¹⁷⁾ of the ith reaction at energy E_n (cm^{-1});

$\phi(E_n)$ is the differential neutron flux at energy E_n (neutrons) ;
 $\text{cm}^2\text{-sec-MeV}$

x is the depth in silicon where the reaction occurs (cm);

- $R_{Ti}(E_n)$ is the range of the particle produced in the i th reaction with a neutron of energy E_n (cm);
- θ is the emission angle from the normal to the detector plane;
- $\frac{\sin \theta}{2}$ is the isotropic emission probability;
- DL is the depletion layer thickness (cm);
- DISC is the low level discriminator setting (MeV);
- $p_s(E_s | x, \theta, R_{Ti}, DL, DISC)$ is the probability of detection of an event given the starting point and direction of the particle, its range, and the depletion layer thickness and discriminator settings. Its value is either 0 or 1, and it serves mainly to shift the recording of an event occurring with a neutron of energy E_n to the channel corresponding to E_s .

The solution procedure is the following:

- 1) For a given neutron energy, the energy of the particle produced, $E_p \cong (E_n + Q_i) \cdot (1 - \text{recoil fraction})$, where the excited level Q value is negative, and the production rate, $\Sigma_i(E_n) \phi(E_n)$, are computed;
- 2) For the particle of energy E_p , the total range in silicon is determined and used to set the upper limit of the x integration, $R_{Ti}(E_n)$;
- 3) For a chosen source distance x and emission

angle θ , the range in each region of each diode, including the two depletion regions, is computed. These distances are related to R_{Ti} , $x/\cos \theta$ and $DL/\cos \theta$;

- 4) Using residual ranges, the energies lost in the two depletion layer regions are calculated. The energy of the recoil is added to the value in the first region;
- 5) If the energies lost in both regions are above the discriminator level, they are added to get the summed particle energy E_s and a $\frac{(\sin \theta)}{2} dx d\theta$ weighted count is placed in the channel corresponding to E_s ;
- 6) The procedure is repeated for all reactions, energies, distances and angles, for the given neutron flux distribution.

5.3 Results and Conclusions.

The above method was applied to the case of an incident Pu- α -Be neutron spectrum, where the Broek-Anderson results⁽¹⁸⁾ were used to represent the spectrum. For this purpose, cross section data for the ground states and excited levels of silicon isotopes, given in Reference 17, were hand fit to obtain sets of curves consistent with the total cross sections. These curves were then used to calculate the expected background contributions from each level of each reaction for the given spectrum. Results of the calculation are given in Figure 20. The background spectrum is seen to be made up of three separate components, one from the $Si^{28}(n,p)$ reaction which is

important in the energy region below 2 MeV, one from the $\text{Si}^{28}(\text{n},\alpha)$ reaction which is important between 2 MeV and 3 MeV, and one from the $\text{Si}^{29}(\text{n},\alpha)$ reaction which is important above 3 MeV. In turn, each of these components is primarily due to the ground state reaction, the excited level reaction counts being shifted to lower energies where they are a small fraction of the total. The true spectrum from a Pu- α -Be source is seen to be obscured by background below a neutron energy of about 3 MeV. On the other hand, for a fission spectrum only the $\text{Si}^{28}(\text{n},\text{p})$ reaction is important and background should always be lower than the true spectrum.

For comparison, available experimental data, taken from Reference 14, are presented in Figure 21. The agreement between the calculated and experimental curves is excellent, both in shape and in absolute magnitude, which proves the validity of the simple model chosen to represent the spectrometer. The fact that the ground state reactions are of primary importance completely explains the discrepancy noted in a previous paper⁽¹¹⁾ between the magnitudes of the true response and the background response.

Acknowledgement.

The author wishes to thank Dr. A.ROTA for helpful discussions during the course of this work.

BIBLIOGRAPHY.

- 1) F.S. ALSMILLER,
"The Distribution in Energy of Alpha-Triton Pairs Resulting from the Neutron Bombardment of Lithium Fluoride",
ORNL - 3016, (1960), 289
- 2) F.S. ALSMILLER,
"The Distribution in Energy of Alpha-Triton Pairs Resulting from the Neutron Bombardment of Lithium Fluoride",
ORNL - 3193, (1961), 119
- 3) R.D. EVANS,
"Passage of Heavy Charged Particles Through Matter",
The Atomic Nucleus, McGraw Hill, (1955), Chapter 22
- 4) S.K. ALLISON, S.D. WARSHAW,
"Passage of Heavy Particles Through Matter",
Revs. Mod. Phys. 25, (1953), 779
- 5) H. BICHSEL,
"Passage of Charged Particles Through Matter",
TID - 18436, (1961)
- 6) R.A. RYDIN,
"Efficiency of a Semiconductor Sandwich Detector in a Flux of Fission Neutrons From a Disk Source",
EUR - 2487. e, (1965)
- 7) R.D. EVANS,
"Conservation Laws for Nuclear Reactions",
The Atomic Nucleus, McGraw-Hill, (1955), Chapter 12
- 8) T.A. LOVE, R.B. MURRAY,
"The Use of Surface-Barrier Diodes for Fast-Neutron Spectroscopy",
IRE ~~Trans.~~ Nucl. Sci., NS-8, (1961), 91

- 9) T.A. LOVE, et al.,
"A Silicon Surface-Barrier Fast-Neutron Spectrometer",
Nuclear Electronics, IAEA, (1962), 415
- 10) T.A. LOVE, K.M.HENRY,
"Fast-Neutron Spectroscopy With Silicon Surface-Barrier
Counters",
ORNL - 3193, (1961), 116
- 11) R.A. RYDIN,
"Design Considerations and Calculations for a Li⁶ Semi-
conductor Sandwich Fast Neutron Spectrometer Experiment",
EUR - 2712. e, (1966)
- 12) M.D. GOLDBERG, et al.,
"Angular Distributions in Neutron-Induced Reactions",
BNL - 400, (1962)
- 13) G.W.R. ENDRES,
"Neutron Spectrum Measurements at Hanford Work Locations",
HW - SA - 3525, (1964)
- 14) E.S. KENNEY,
"A Semiconductor Detector Fast Neutron Spectrometer",
TID - 21202, (1962)
- 15) M.G. SILK,
"Attempts to Determine the Fast-Neutron Spectrum in a
Thermal Reactor by Means of Li⁶ and He³ Semiconductor
Spectrometers",
AERE - M 1590, (1965)
- 16) R.GOLD,
"An Iterative Unfolding Method for Response Matrices",
ANL - 6984; (1964)
- 17) J.R. STEHN et al.,
"Neutron Cross Sections Vol I, Z = 1 to 20",
BNL - 325 Second Edition (Supplement 2), (1964)

- 18) H.W. BROEK, C.E. ANDERSON,
"The Stilbene Scintillation Crystal as a Spectrome-
ter for Continuous Fast-Neutron Spectra",
Rev. Sci. Inst. 31, (1960), 1063

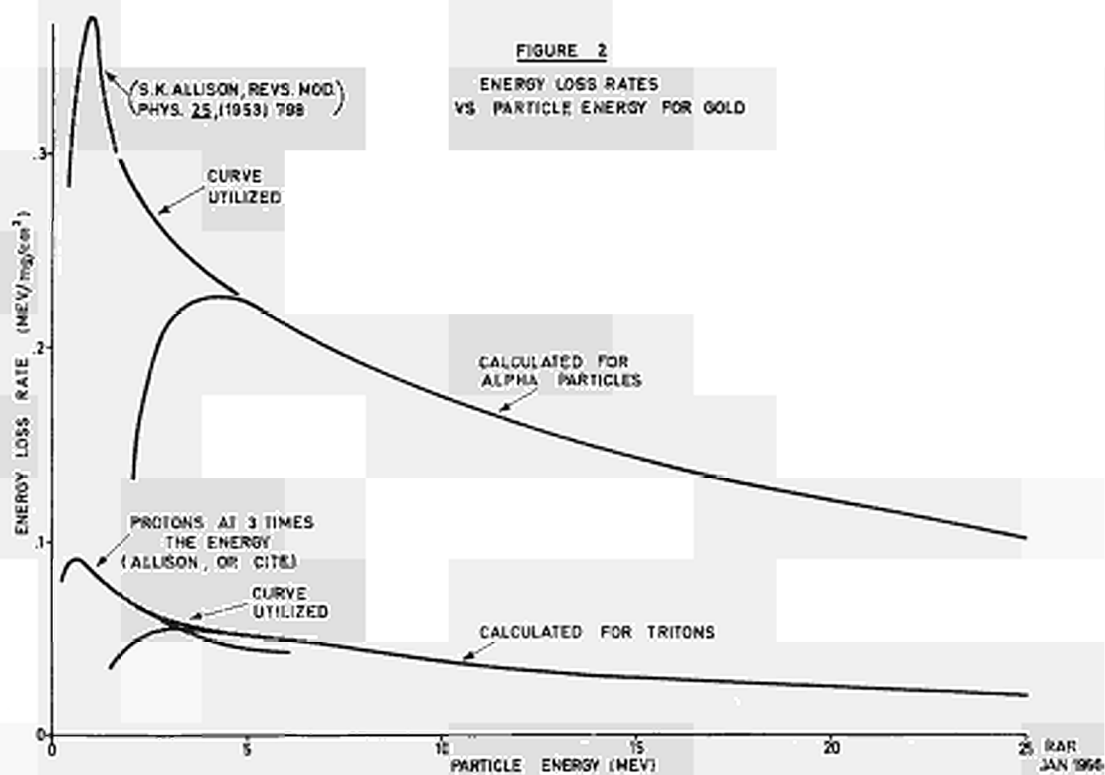
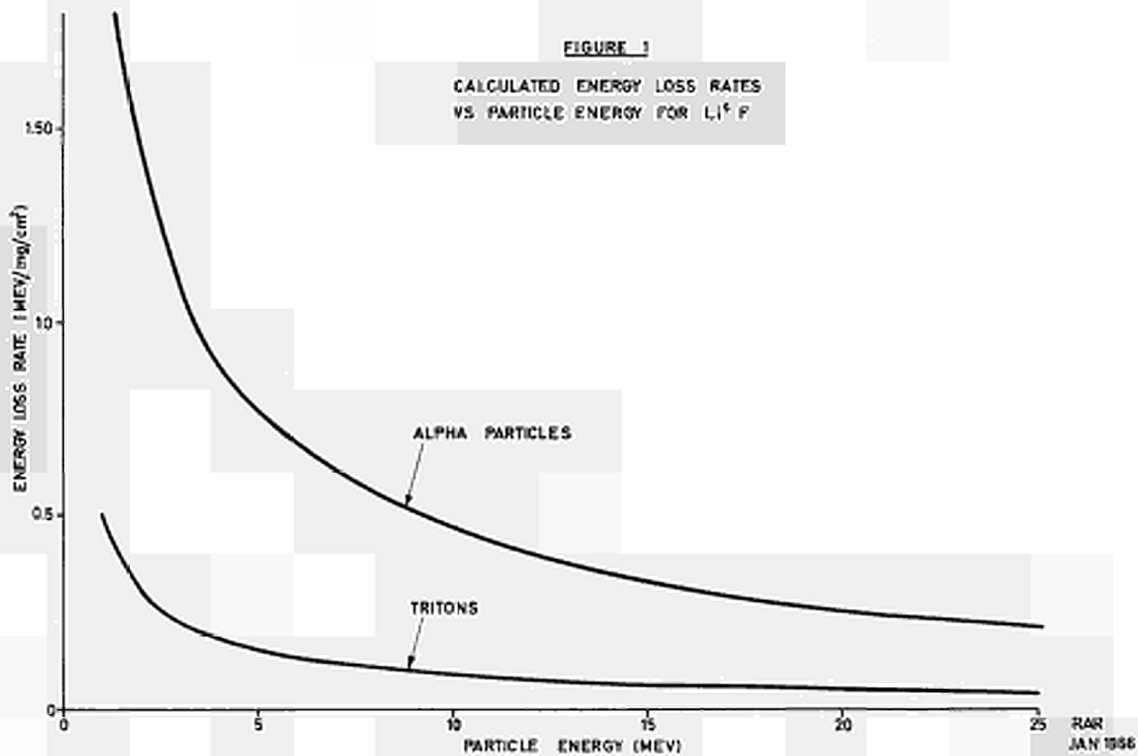
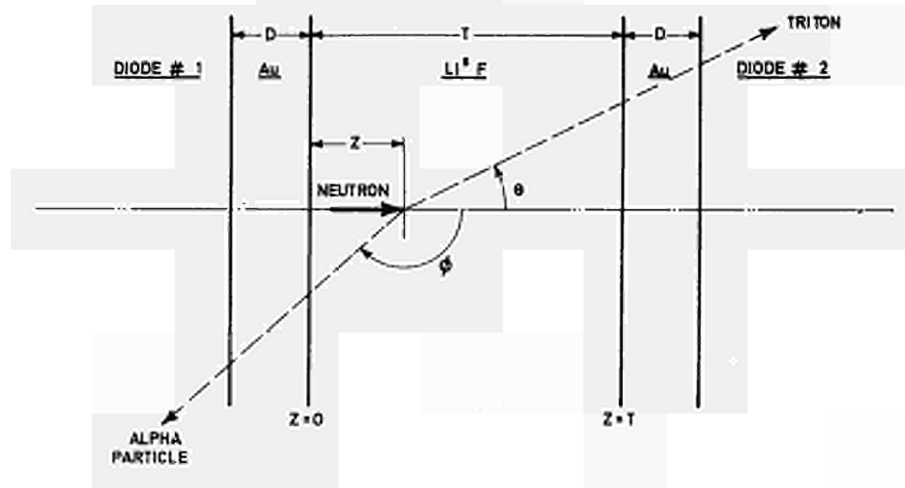


FIGURE 3

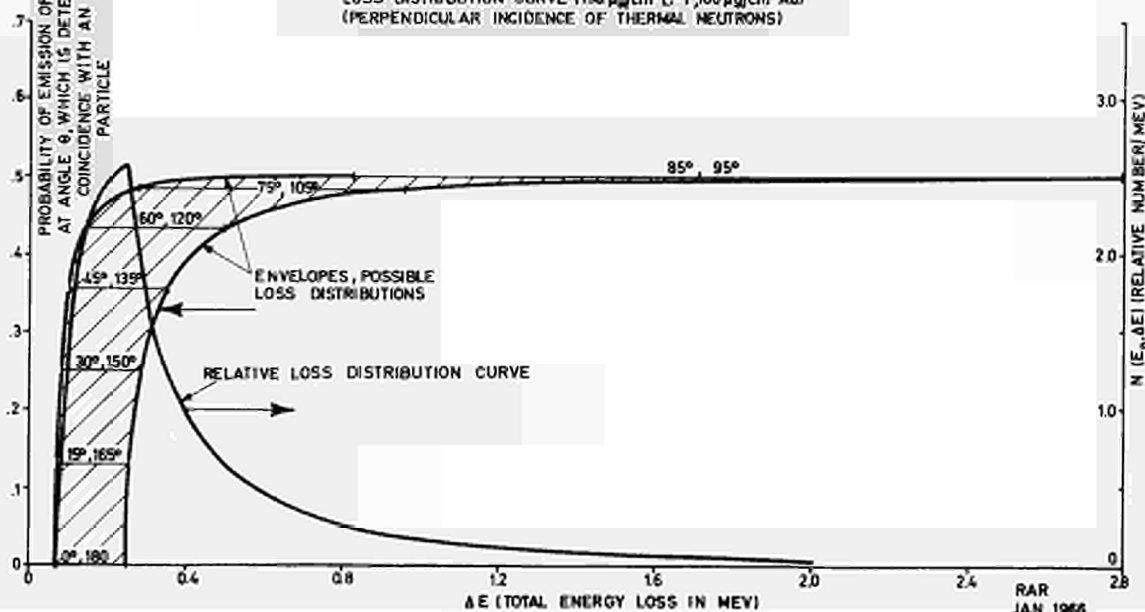
GEOMETRY FOR THE CALCULATION OF THE CHARACTERISTIC RESOLUTION FUNCTION OF A SEMICONDUCTOR SANDWICH SPECTROMETER



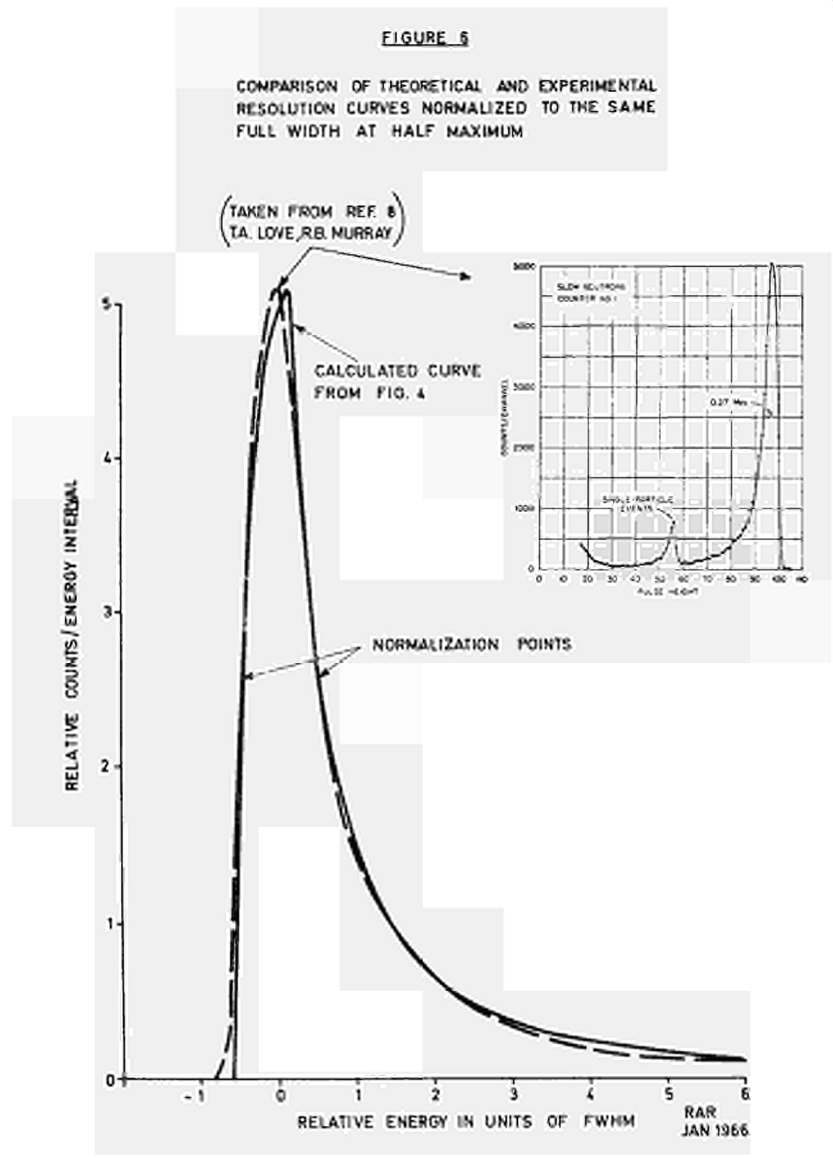
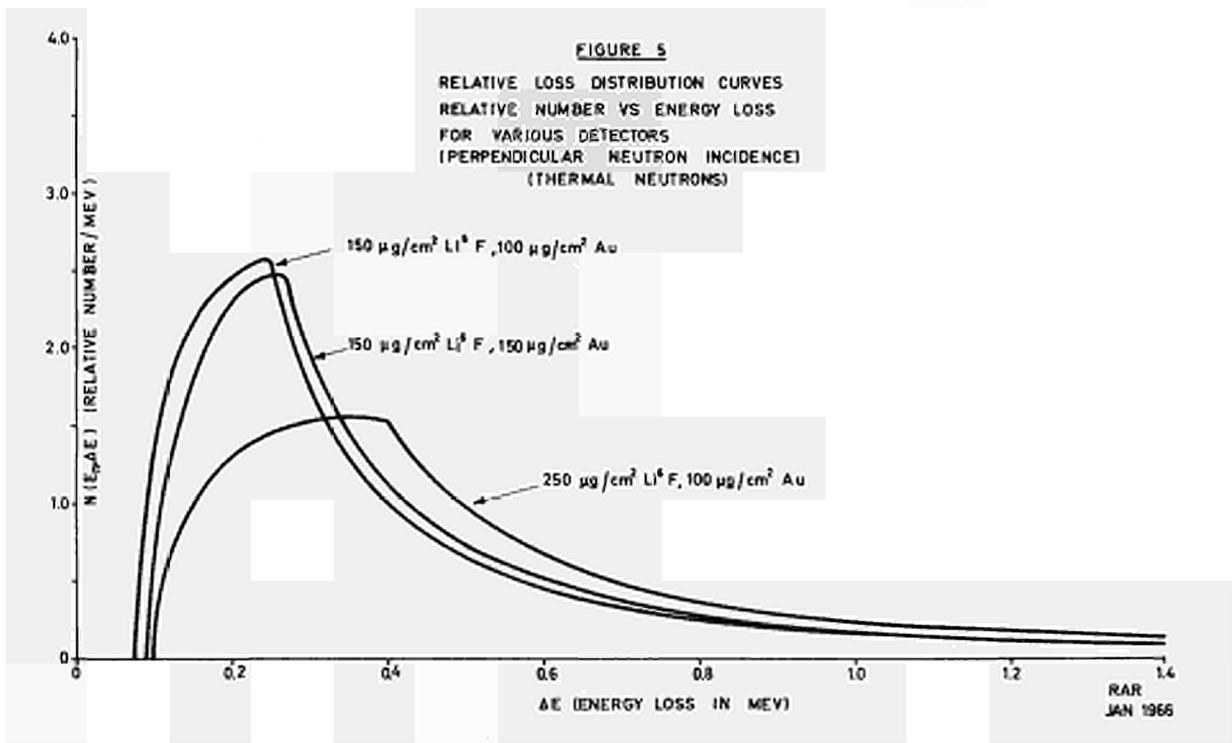
RAR
JAN 1966

FIGURE 4

LOSS DISTRIBUTION PROBABILITIES VS ENERGY LOSS FOR VARYING TRITON EMISSION ANGLE, RELATIVE LOSS DISTRIBUTION CURVE ($1150 \mu g/cm^2 LiF, 100 \mu g/cm^2 Au$) (PERPENDICULAR INCIDENCE OF THERMAL NEUTRONS)



RAR
JAN 1966



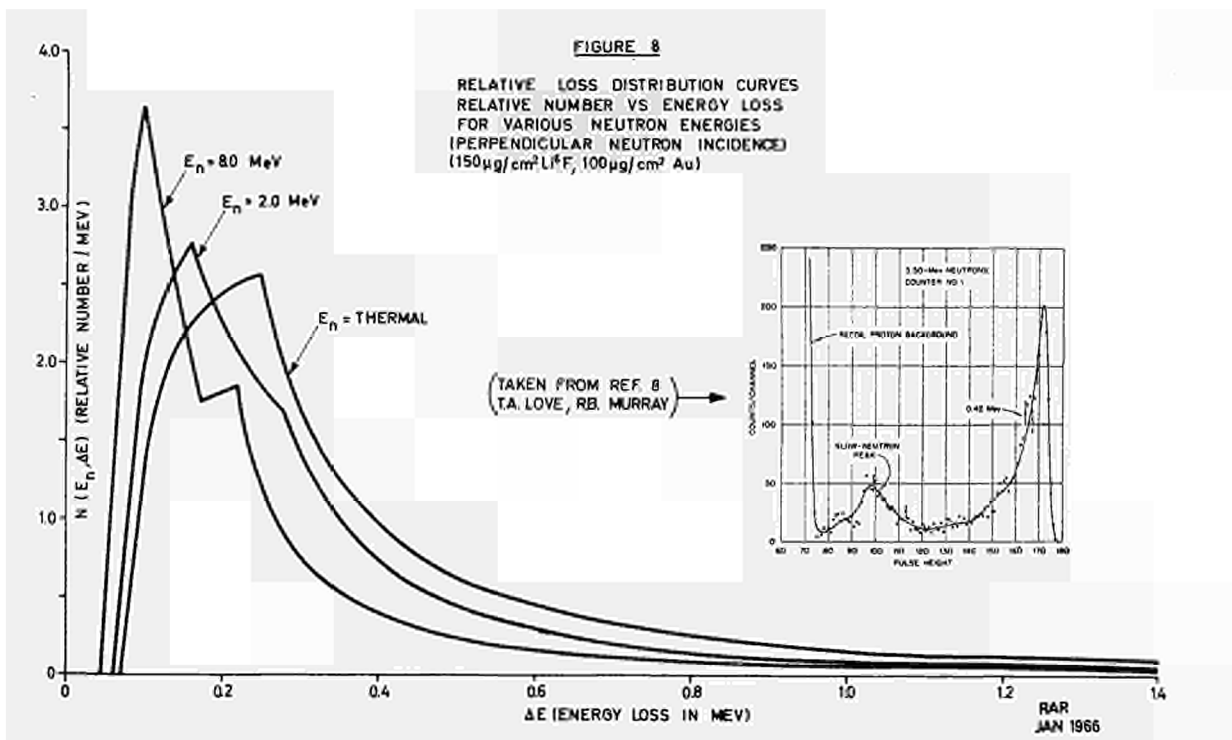
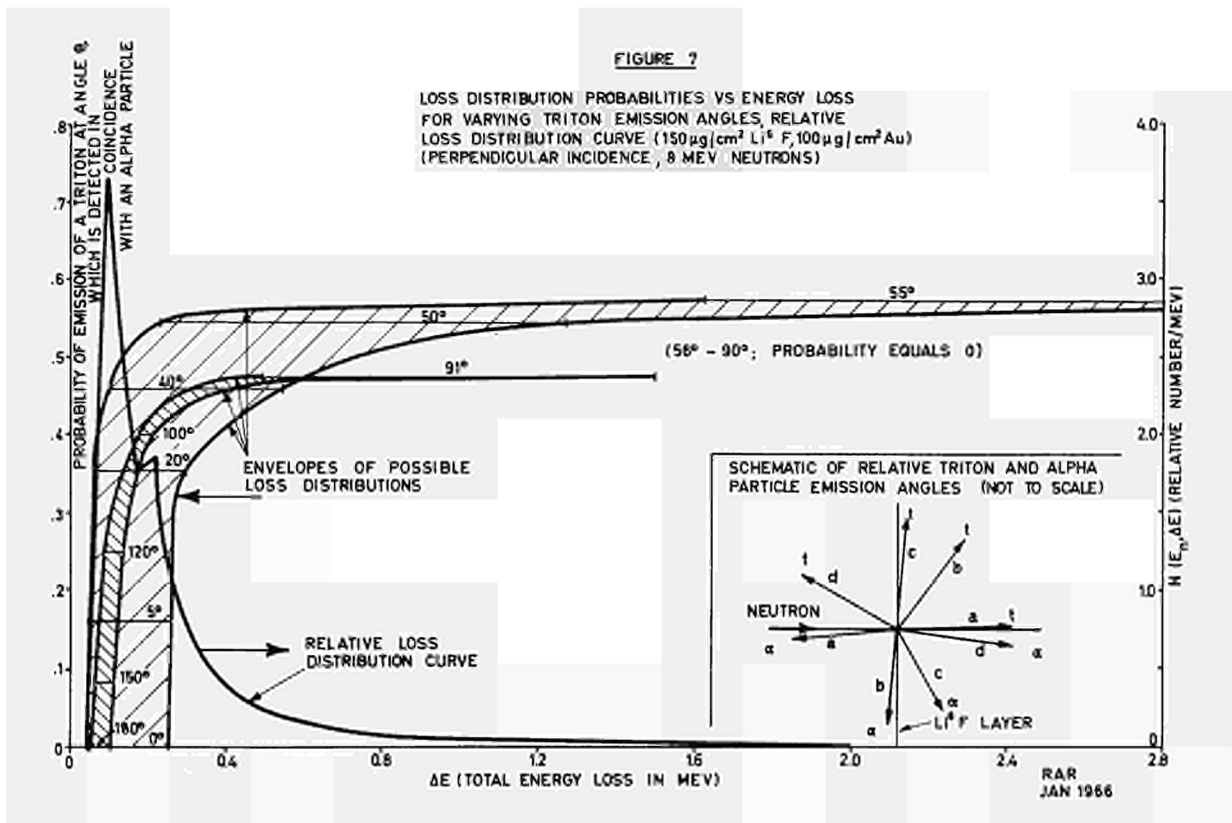
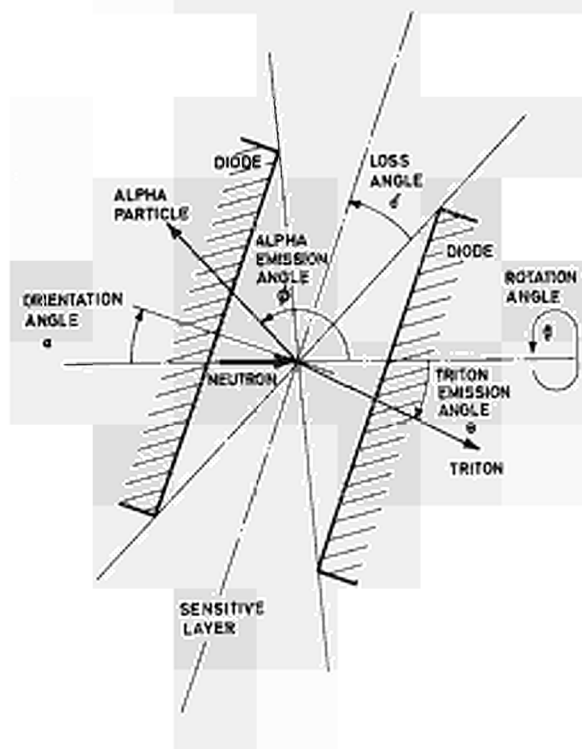


FIGURE 9

DETECTION CONDITIONS FOR
A SEMICONDUCTOR SANDWICH DETECTOR



RAR
JAN 1966

FIGURE 10

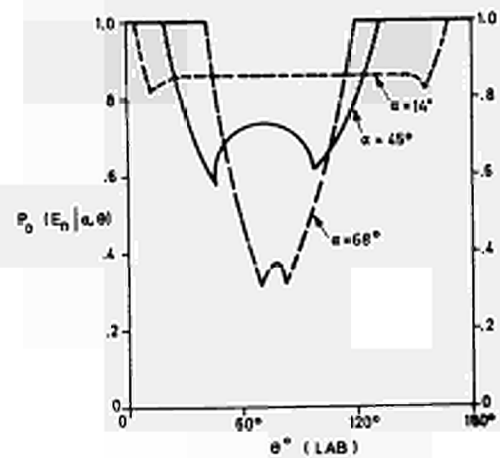
CONDITIONAL DETECTION PROBABILITY

$$P_D(E_n | \alpha, \theta) \text{ VS } \theta_{\text{LAB}} (\text{TRITON})$$

$$E_n = 10 \text{ MEV}$$

$$\phi = 0^\circ$$

$$\text{Li}^6(n, T)$$



RAR
JAN 1966

FIGURE 11

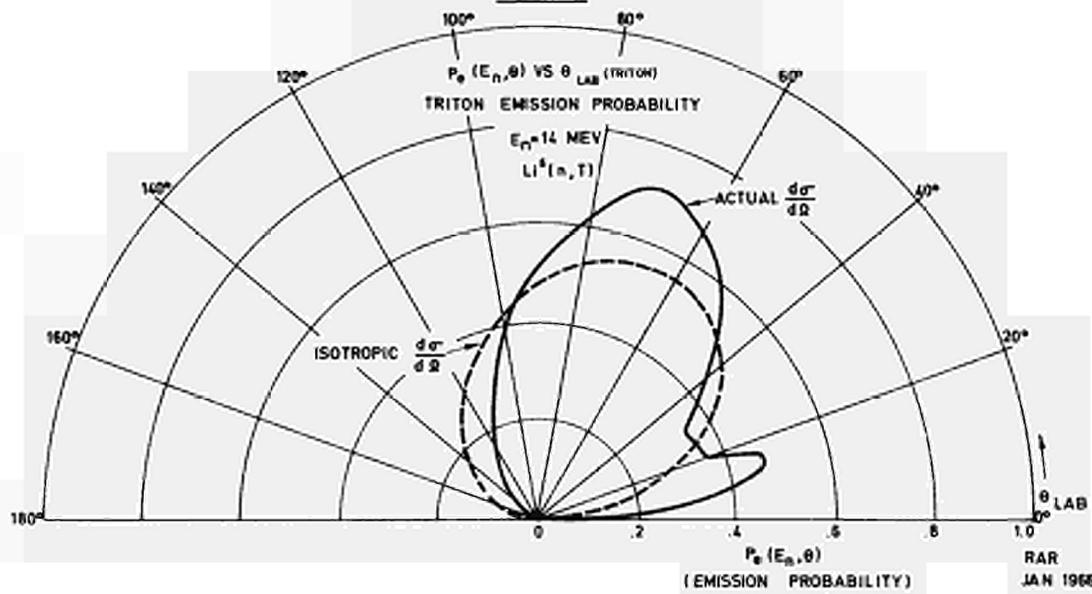


FIGURE 12

Li^6 SEMICONDUCTOR SANDWICH DETECTOR, RELATIVE
 DETECTION EFFICIENCY VS ENERGY FOR VARIOUS
 DETECTOR ORIENTATIONS WITH RESPECT TO THE NEUTRON BEAM
 (NO DISCRIMINATION OF THERMAL NEUTRON EVENTS)

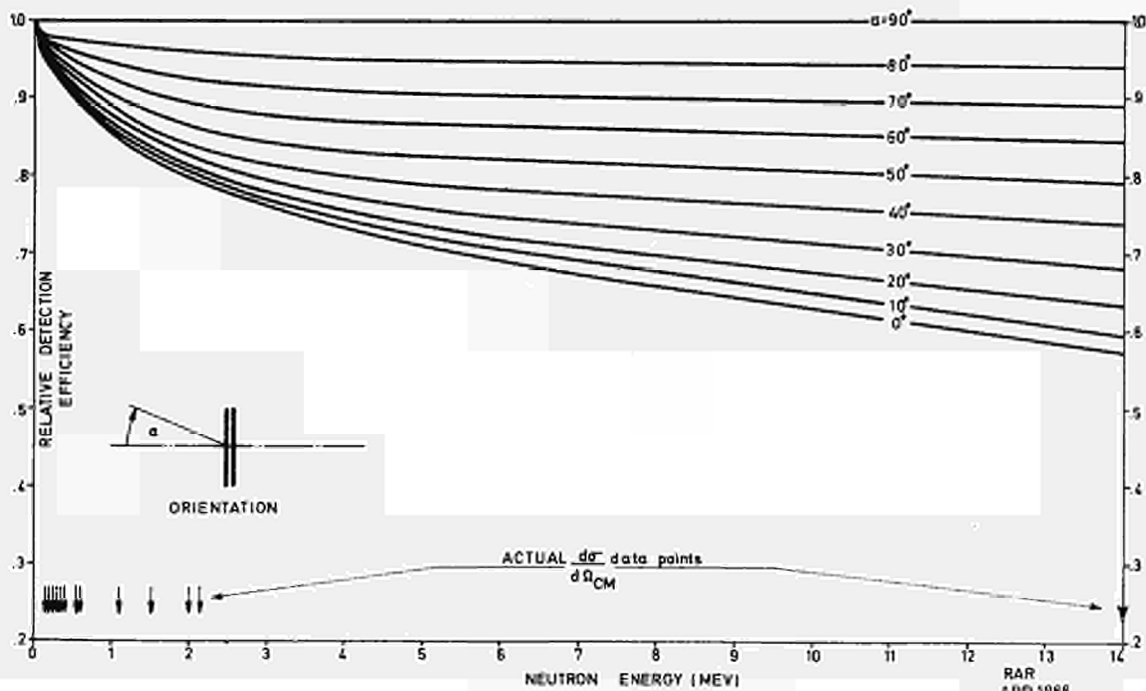


FIGURE 13

Li^6 SEMICONDUCTOR SANDWICH DETECTOR, RELATIVE DETECTION EFFICIENCY VS ENERGY FOR VARIOUS DETECTOR ORIENTATIONS WITH RESPECT TO THE NEUTRON BEAM (DISCRIMINATOR = 21 MEV)

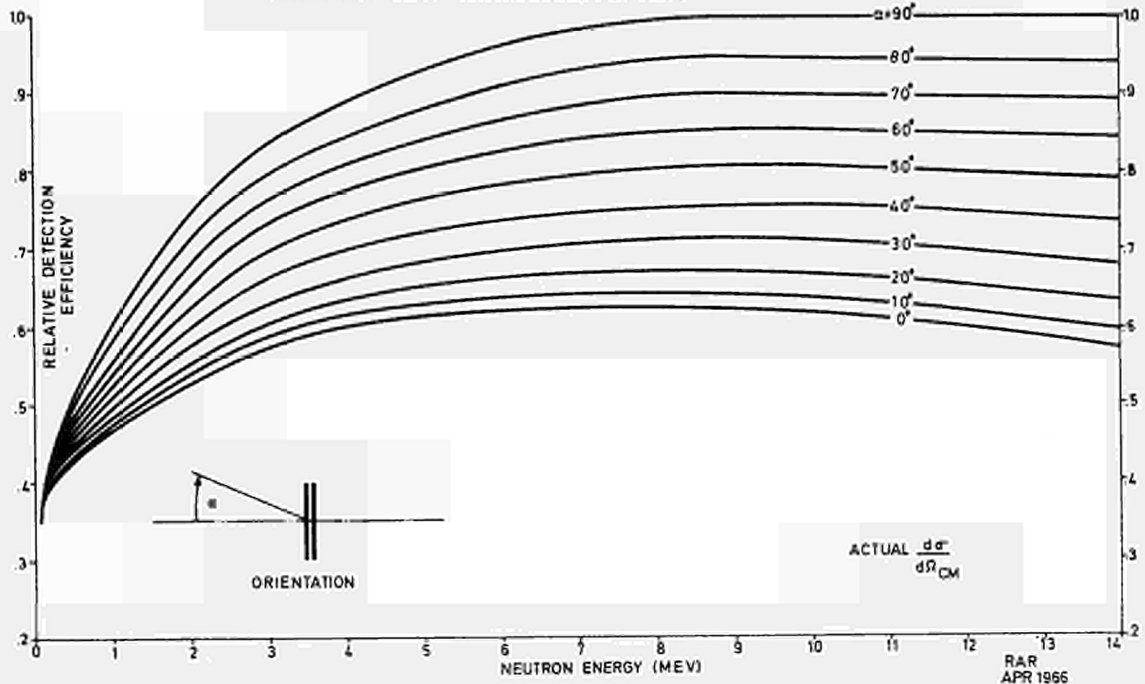


FIGURE 14

He^3 SEMICONDUCTOR SANDWICH DETECTOR, RELATIVE DETECTION EFFICIENCY VS ENERGY FOR VARIOUS DETECTOR ORIENTATIONS WITH RESPECT TO THE NEUTRON BEAM (NO DISCRIMINATION OF THERMAL NEUTRON EVENTS, LOSS ANGLE $\delta = 0^\circ$)

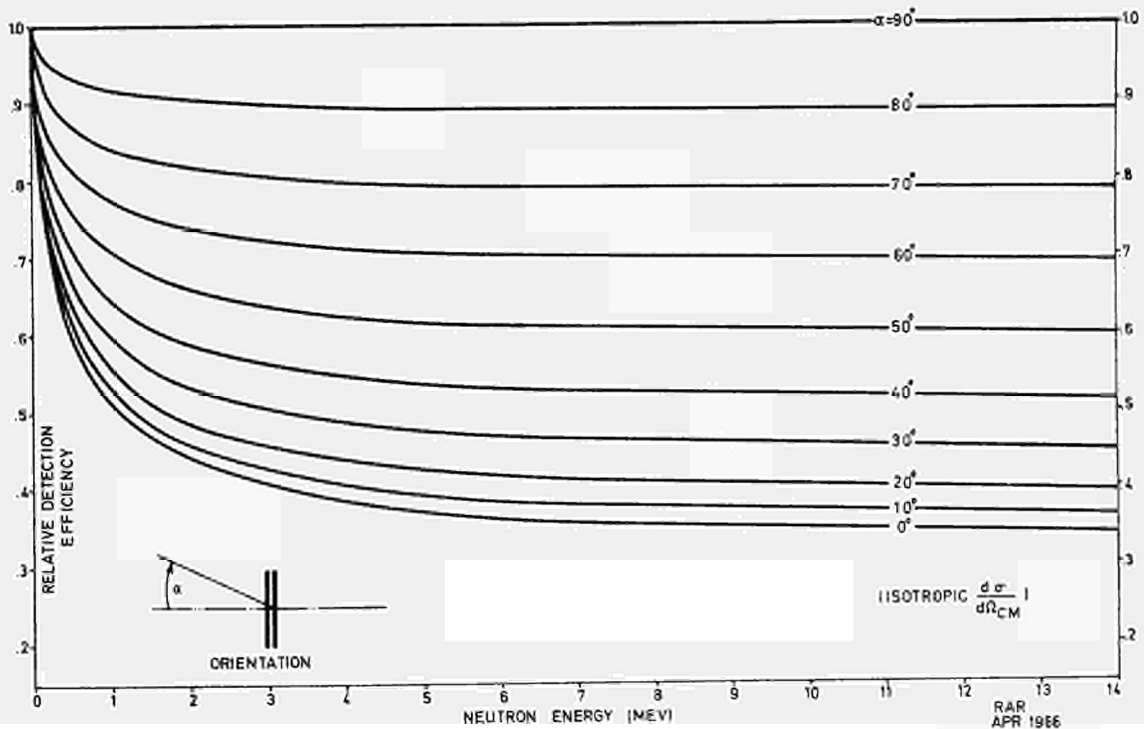


FIGURE 15

He^3 SEMICONDUCTOR SANDWICH DETECTOR, RELATIVE DETECTION EFFICIENCY VS ENERGY FOR VARIOUS DETECTOR ORIENTATIONS WITH RESPECT TO THE NEUTRON BEAM (NO DISCRIMINATION OF THERMAL NEUTRON EVENTS, LOSS ANGLE $\delta = 5^\circ$)

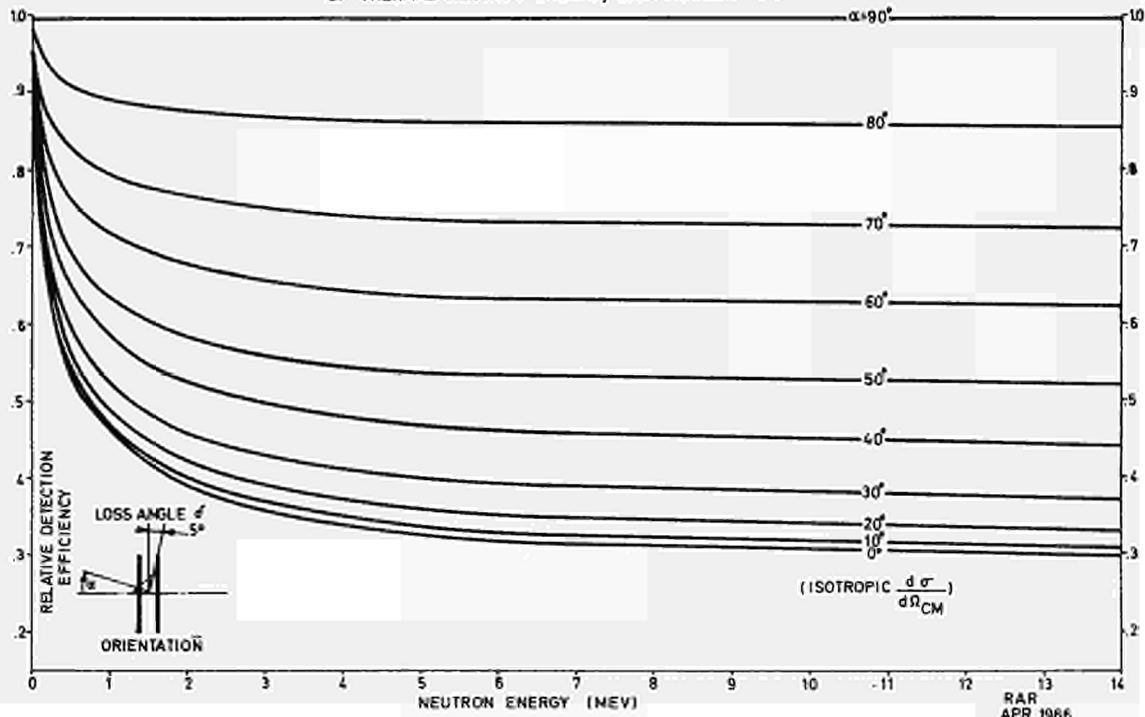


FIGURE 16

He^3 SEMICONDUCTOR SANDWICH DETECTOR, RELATIVE DETECTION EFFICIENCY VS ENERGY FOR VARIOUS DETECTOR ORIENTATIONS WITH RESPECT TO THE NEUTRON BEAM (NO DISCRIMINATION OF THERMAL NEUTRON EVENTS, LOSS ANGLE $\delta = 10^\circ$)

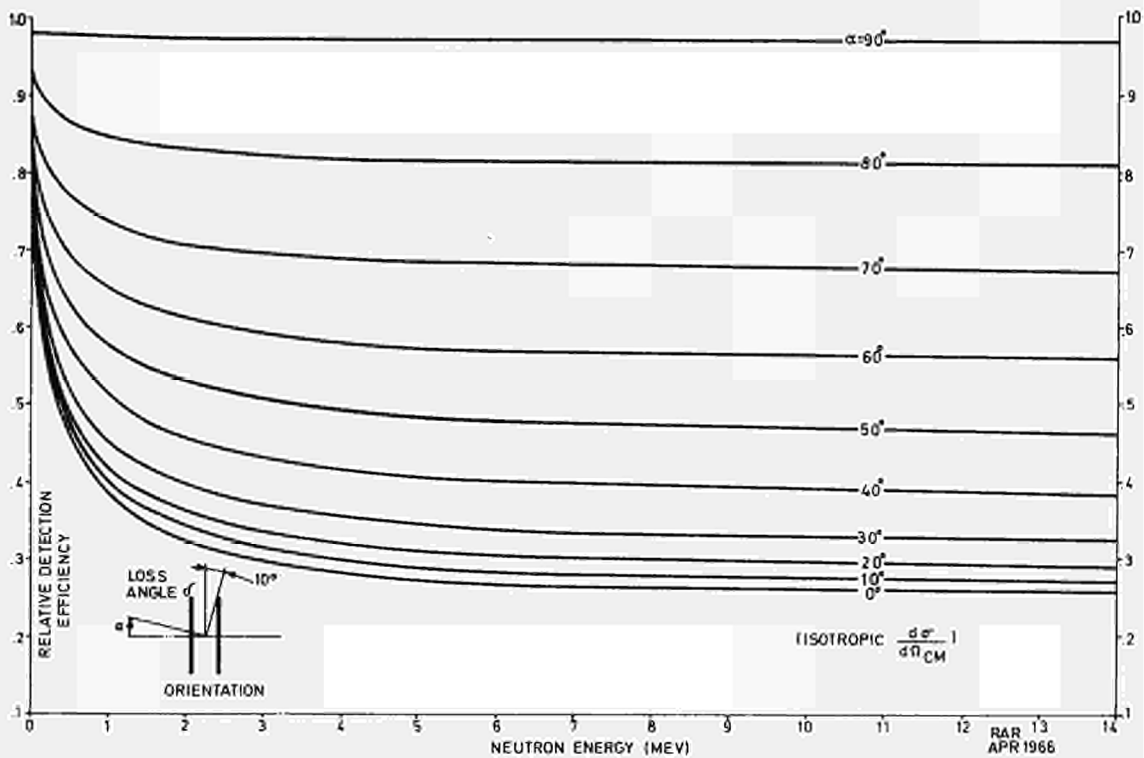


FIGURE 17

He^3 SEMICONDUCTOR SANDWICH DETECTOR, RELATIVE DETECTION EFFICIENCY VS ENERGY FOR VARIOUS DETECTOR ORIENTATIONS WITH RESPECT TO THE NEUTRON BEAM (DISCRIMINATOR SET AT 0.2 MEV)

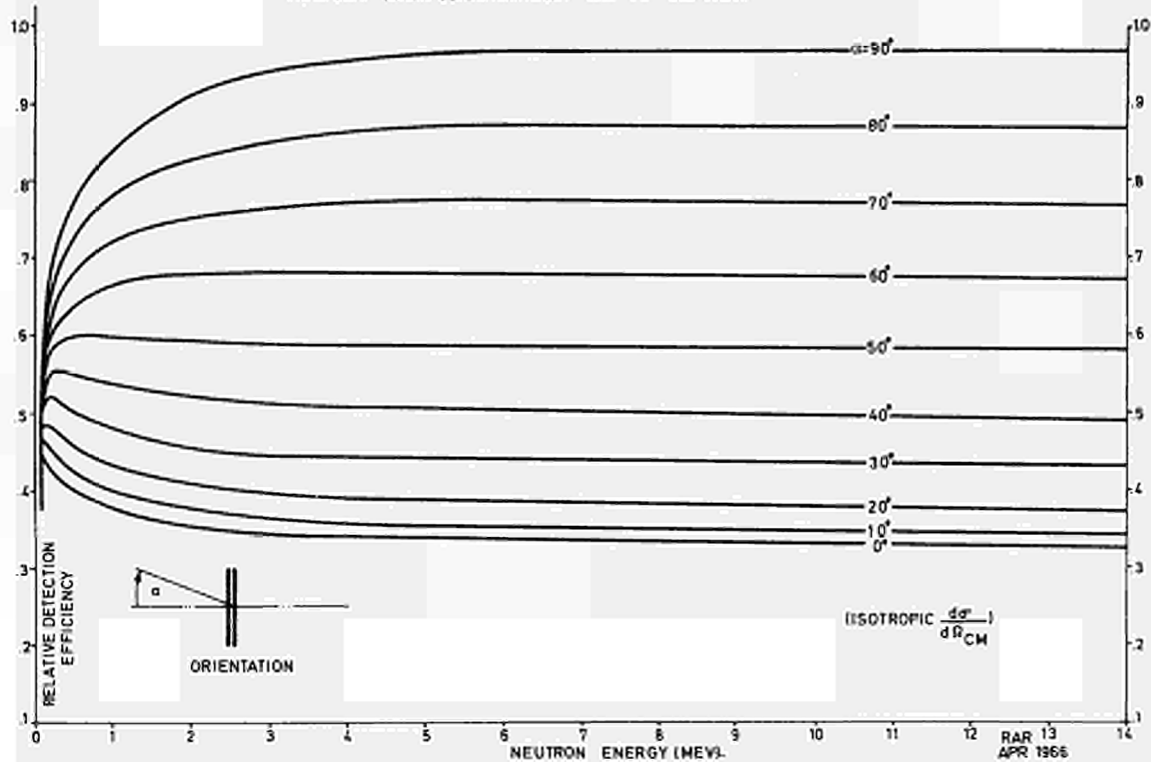
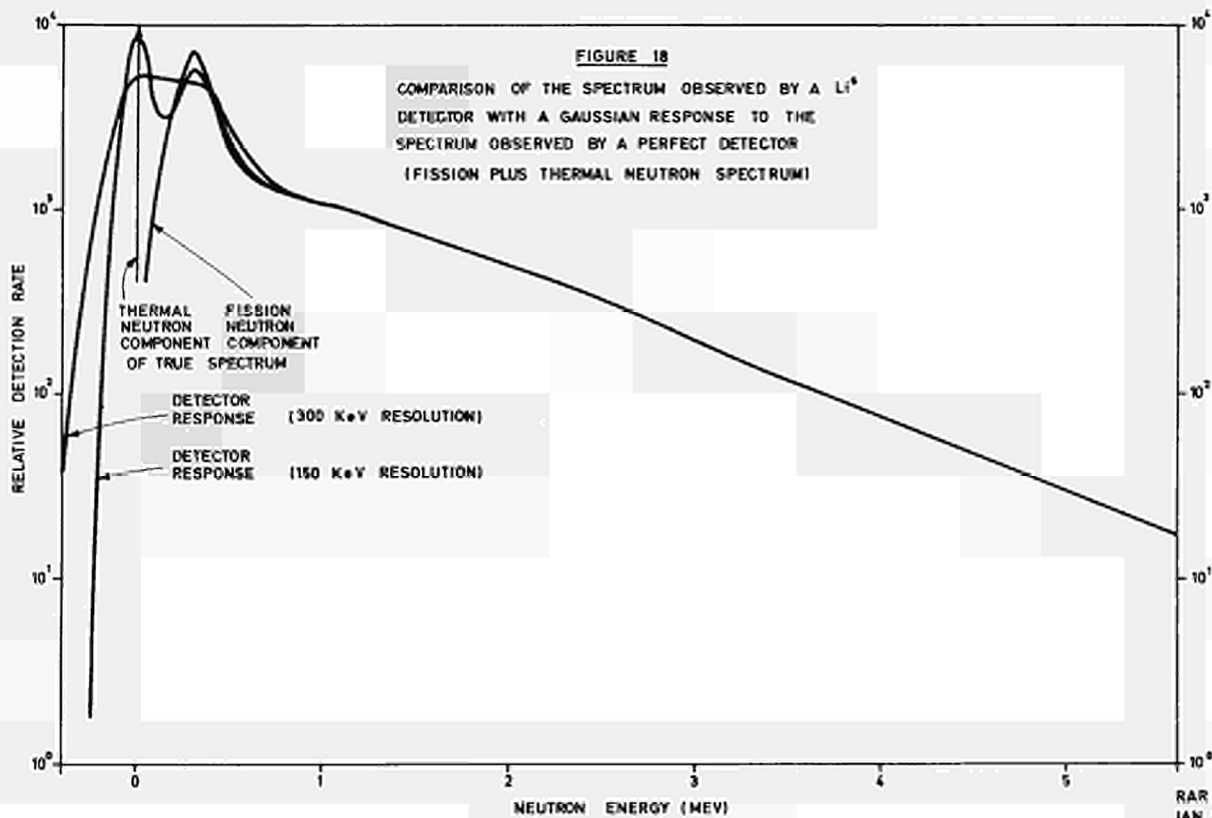
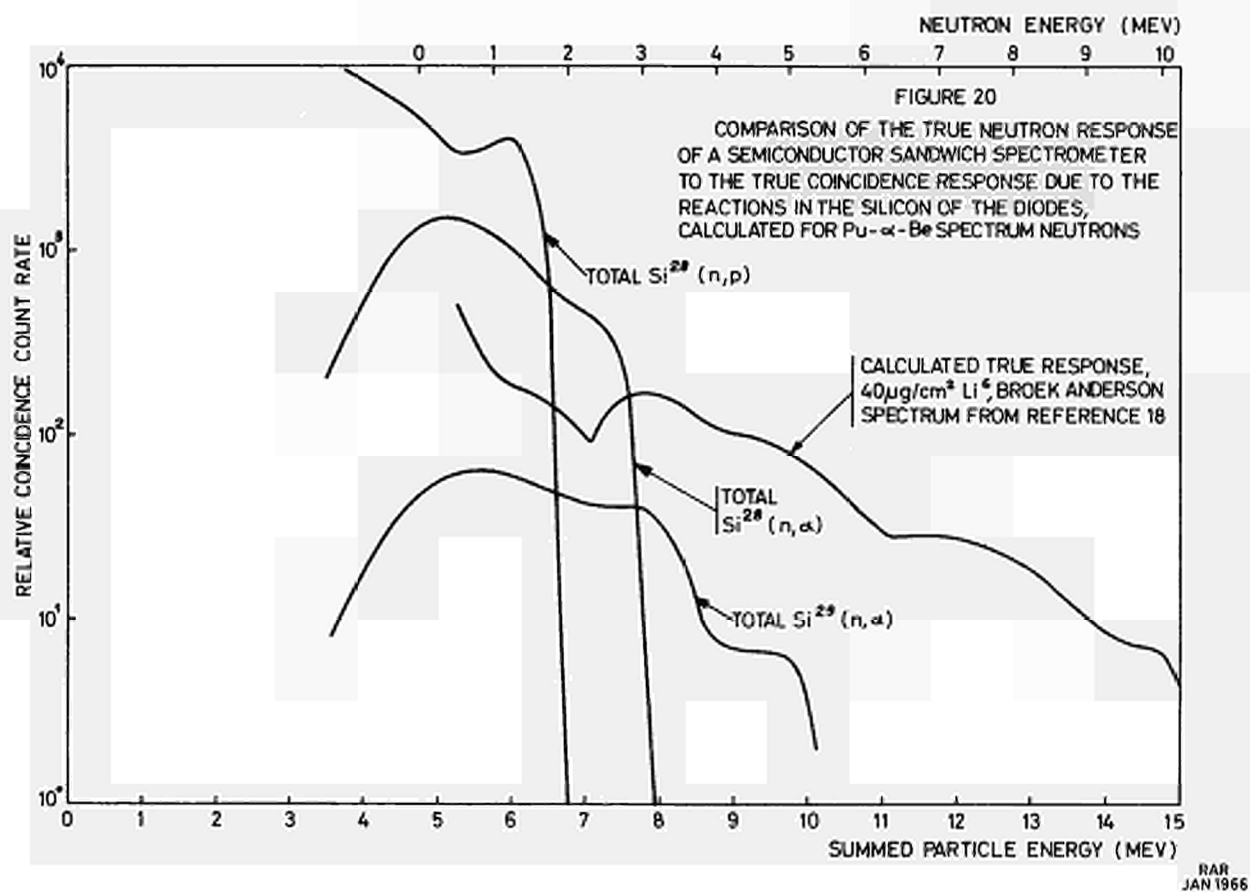
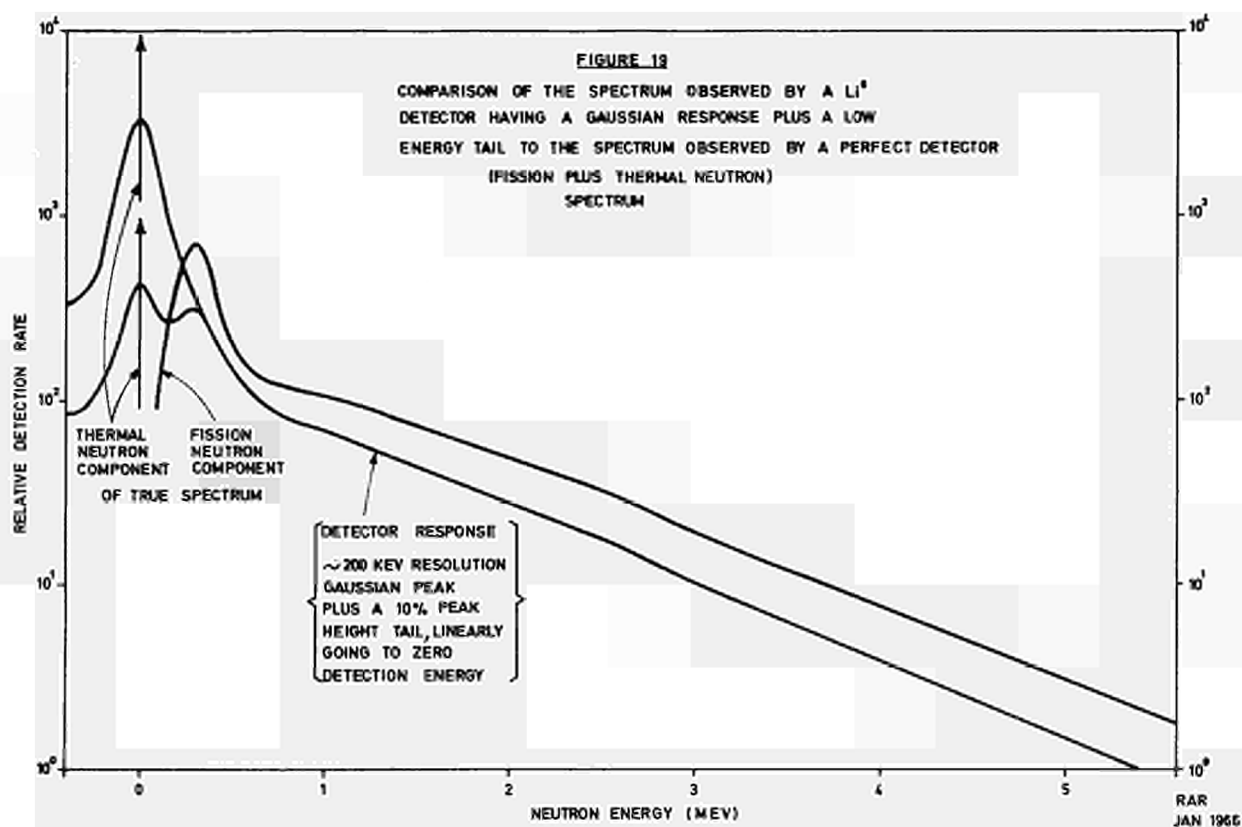
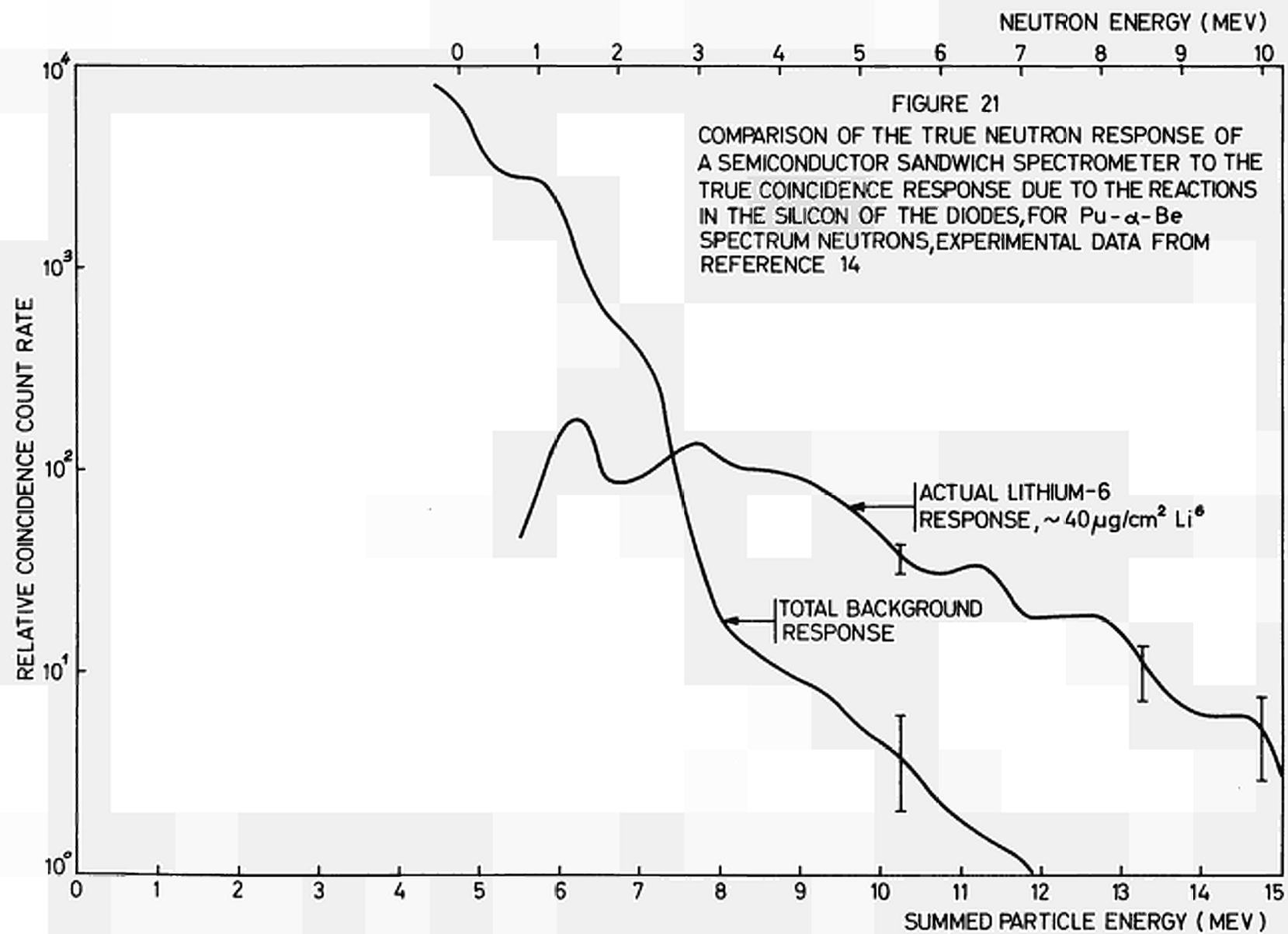


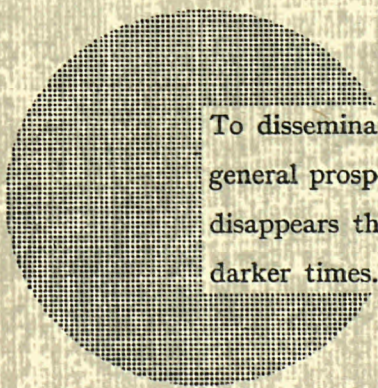
FIGURE 18

COMPARISON OF THE SPECTRUM OBSERVED BY A Li^6 DETECTOR WITH A GAUSSIAN RESPONSE TO THE SPECTRUM OBSERVED BY A PERFECT DETECTOR (FISSION PLUS THERMAL NEUTRON SPECTRUM)









To disseminate knowledge is to disseminate prosperity — I mean general prosperity and not individual riches — and with prosperity disappears the greater part of the evil which is our heritage from darker times.

Alfred Nobel

SALES OFFICES

All Euratom reports are on sale at the offices listed below, at the prices given on the back of the cover (when ordering, specify clearly the EUR number and the title of the report, which are shown on the cover).

PRESSES ACADEMIQUES EUROPEENNES

98, Chaussée de Charleroi, Bruxelles 6

Banque de la Société Générale - Bruxelles
compte N° 964.558,

Banque Belgo Congolaise - Bruxelles
compte N° 2444.141,

Compte chèque postal - Bruxelles - N° 167.37,

Belgian American Bank and Trust Company - New York
compte No. 22.186,

Lloyds Bank (Europe) Ltd. - 10 Moorgate, London E.C.2,
Postcheckkonto - Köln - Nr. 160.861.

CDNA02994ENC

OFFICE CENTRAL DE VENTE DES PUBLICATIONS DES COMMUNAUTES EUROPEENNES

2, place de Metz, Luxembourg (Compte chèque postal N° 191-90)

BELGIQUE — BELGIË

MONITEUR BELGE
40-42, rue de Louvain - Bruxelles
BELGISCH STAATSBAD
Leuvenseweg 40-42 - Brussel

GRAND-DUCHE DE LUXEMBOURG

OFFICE CENTRAL DE VENTE
DES PUBLICATIONS DES
COMMUNAUTES EUROPEENNES
9, rue Goethe - Luxembourg

DEUTSCHLAND

BUNDESANZEIGER
Postfach - Köln 1

ITALIA

LIBRERIA DELLO STATO
Piazza G. Verdi, 10 - Roma

FRANCE

SERVICE DE VENTE EN FRANCE
DES PUBLICATIONS DES
COMMUNAUTES EUROPEENNES
26, rue Desaix - Paris 15^e

NEDERLAND

STAATSDRUKKERIJ
Christoffel Plantijnstraat - Den Haag

EURATOM — C.I.D.
51-53, rue Belliard
Bruxelles (Belgique)